ADVANCES IN ATMOSPHERIC SCIENCES, VOL. 29, NO. 5, 2012, 1089–1099

Satellite-Based Monitoring of Decadal Soil Salinization and Climate Effects in a Semi-arid Region of China

WANG Hesong (王鹤松) and JIA Gensuo* (贾根锁)

Key Laboratory of Regional Climate-Environment Research for East Asia,

Institute of Atmospheric Physics, Chinese Academy of Sciences, Beijing 100029

(Received 10 August 2011; revised 22 December 2011)

ABSTRACT

Soil salinization is a common phenomenon that affects both the environment and the socio-economy in arid and semi-arid regions; it is also an important aspect of land cover change. In this study, we integrated multi-sensor remote sensing data with a field survey to analyze processes of soil salinization in a semi-arid area in China from 1979 to 2009. Generally, the area of salt-affected soils increased by 0.28% per year with remarkable acceleration from 1999 to 2009 (0.42% increase per year). In contrast, the area of surface water bodies showed a decreasing trend (−0.08% per year) in the same period. Decreases in precipitation and increases in aridity due to annual (especially summer) warming provided a favorable condition for soil salinization. The relatively flat terrain favored waterlogging at the surface, and continuous drought facilitated upward movement of soil water and accumulation of surface saline and calcium. Meanwhile, land-use practices also played a crucial role in accelerating soil salinization. The conversion to cropland from natural vegetation greatly increased the demand for groundwater irrigation and aggravated the process of soil salinization. Furthermore, there are potential feedbacks of soil salinization to regional climate. The salinization of soils can limit the efficiency of plant water use as well as photosynthesis; therefore, it reduces the amount of carbon sequestrated by terrestrial ecosystem. Soil salinization also reduces the absorbed solar radiation by increasing land surface albedo. Such conversions of land cover significantly change the energy and water balance between land and atmosphere.

Key words: soil salinization, land cover change, remote sensing, semi-arid China, land–atmosphere interactions

Citation: Wang, H. S., and G. S. Jia, 2012: Satellite-based monitoring of decadal soil salinization and climate effects in a semi-arid region of China. *Adv. Atmos. Sci.*, **29**(5), 1089–1099, doi: 10.1007/s00376-012-1150-8.

1. Introduction

Soil salinization refers to surface or near-surface accumulation of salts, mainly chlorides, sulfates, and carbonates of sodium, calcium, and magnesium (Shrestha, 2006). Salt is a critical constraint to terrestrial ecosystem production and even the local economy in arid and semi-arid regions where potential evaporation greatly exceeds precipitation (Wang et al., 2007). Soil salinization is also an important aspect of land cover change. Globally, primary salt-affected soils cover ∼955 Mha, while secondary salinization affects ∼77 Mha (Metternicht and Zinck, 2003). Soil salinization is a worldwide environmental problem and one of the main types of soil degradation phenomena in arid and semi-arid regions (Metternicht and Zinck, 2003; Fernandez-Buces et al., 2006). Soil salinization can exert great environmental pressure on terrestrial ecosystems in semi-arid regions because these areas under harsh climatic conditions are also under high pressure to supply the required food for their rapidly increasing population (Farifteh et al., 2006). Many previous studies have indicated that soil salinization in arid and semi-arid regions has accelerated in recent years (Ma-

*Corresponding author: JIA Gensuo, jiong@tea.ac.cn

soud and Koike, 2006; Li et al., 2007; Chen and Rao, 2008).

The semi-arid region of China, mainly located in northern China, is one of the regions most seriously affected by soil salinization. This region is also one of the main dryland grain production and pasturing areas in the world, and it has an important role in the State grain storage and food security system (Chen and Rao, 2008). Because of economic development and increasing population, environmental degradation related to land use is becoming intense enough to constitute a severe threat to regional sustainable development (Qi and Luo, 2006). Soil salinization has become a major environmental problem and a key issue affecting the sustainable development of the region (Wang et al., 2008). Generally, the dynamics of soil salinization in semi-arid China are largely related to cultivation of natural grassland, irrigation, and industrial development (Li et al., 2007; Chen and Rao, 2008).

Mapping and tracking the spatial and temporal change of salt-affected soil areas is necessary for fully understanding the process of soil salinization and resource management. Accurate assessment of the status of, changes in, and trends in soil salinization ensures that critical information is available for the development of strategies to mitigate this important problem (Yang et al., 2005). Remotely sensed detection of dynamic change is a widely used method for monitoring the land surface. Many studies have utilized remote sensing techniques to monitor, classify, and depict the process of soil salinization (Metternicht and Zinck, 1997; Abuzar et al., 2001; Howari, 2003; Farifteh et al., 2007; Lobell et al., 2007; Eldeiry and Garcia, 2008). Unfortunately, few have focused on soil salinization and its feedback to climate. Because land cover changes have an important role in climate change, soil salinization has become critical in semi-arid China. Monitoring the process of soil salinization and evaluating its influence on regional climate are badly needed.

Remote sensing is one of the most efficient methods of environmental monitoring; it is widely recognized as an effective and efficient tool for collecting information on interannual changes in land-surface properties, including soil salinization. Meanwhile, field survey activities are indispensable for interpreting "ground truth" information, identifying critical categories for satellite data classification, and collecting local interrelated information regarding geology, vegetation, climate, soils, and land use (Funakawa and Kosaki, 2003).

In this study, we utilized an integrated method of remote sensing combined with field surveys to monitor soil salinization in the Tongyu region, a typical area being seriously affected by soil salinization in the semi-arid region of China. In the following sections of this article, features and types of soil salinization are identified, and the driving factors behind soil salinization are also discussed. Finally, the influence of soil salinization on climate in terms of terrestrial ecosystem production and energy budget are evaluated.

2. Study area

The study area is located in the western part of the Songnen Plain, in central northeast China; it covers 8496 km^2 (Fig. 1). Songnen Plain lies between 43°36′N to 49°45′N and 121°27′E to 128°12′E. It is not only an important grain production base in China, but it is also one of the three areas of saline–sodic soils in the world (Zhang et al., 2007). Large areas in this region are affected by soil salinization, which has threatened dry-land grain production in recent years (Chen and Zhou, 2005). We chose the Tongyu region as a study area because it represents a typical salt-affected area, and it hosts two *in situ* flux towers of the Coordinated Energy and Water Cycle Observations Project (CEOP, http://www.ceop.net/), an international project that monitors long-term changes of energy and water flux between the land surface and the atmosphere.

The soil types of Tongyu are the following: light chernozem, sandy, meadow, saline and alkali soils. The climate of Tongyu belongs to a continental monsoon climate and semi-arid climate. Groundwater is a primary water resource for agricultural and other uses. In the past 30 years, the mean annual temperature is ∼6.0°, the mean annual precipitation is ∼369 mm, and the mean annual potential evaporation is ∼1015 mm. Rainfall events from June to August account for ∼72% of the annual precipitation.

3. Data and methodology

3.1 *Field data collection and survey*

Dominant land cover categories identified on the satellite image were chosen to define lines for our field survey in October 2008 and July 2009. These main land cover types in this area were considered croplands, grasslands, woodlands, residential areas, salt-affected soils, water bodies, and wetlands. We took transect measurements with a GPS, a digital camera, and an ASD (Analytical Spectral Devices) spectrometer to help us better classify land cover types with remote sensing images. The field data collected were then summarized and analyzed to create training pixels for subsequent supervised classification of satellite data. Local historical information about the change of land use, grazing intensity, and frequency of flood were collected by visiting local inhabitants and refer-

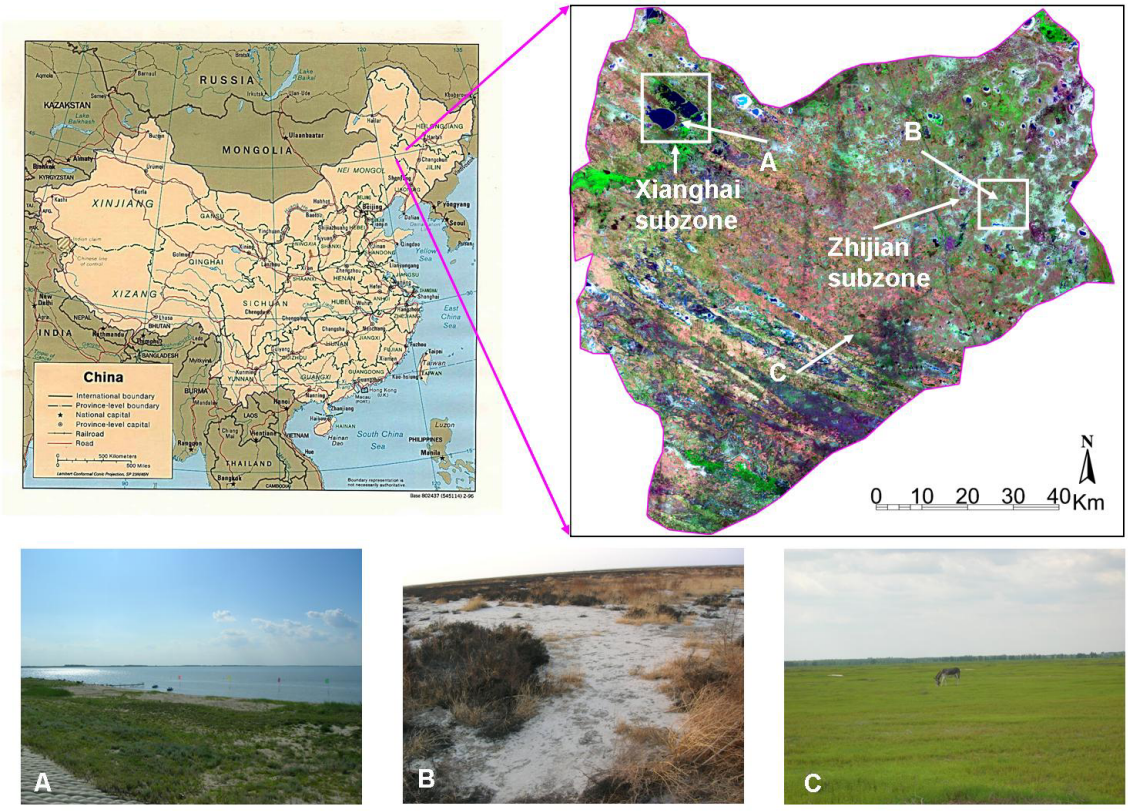

Fig. 1. Location of the study area. The map of the study area was generated from three bands (7, 4, 2 for RGB, respectively) for July 2009 TM5. The typical sites in the study area were surveyed on October 2008 and July 2009. (A) Grasslands and water body, (B) salt-affected soils, (C) grasslands.

ring to local statistical data. The acquisition data were overlapped over Landsat images for subsequent spatial analysis.

Aridity index (AI) was employed to analyze dry and wet variation of the study area:

$$\mathrm{AI} = P/\mathrm{PE}\,, \tag{1}$$

where AI is the aridity index, P is precipitation, and PE is potential evaporation calculated using Penman's method (Penman, 1948).

3.2 *Multi-sensor satellite data*

Continuous observations offered by Landsat satellite images enabled our study of dynamic changes in land surface driven by both natural and human disturbances. The Shuttle Radar Topography Mission (SRTM) obtained elevation data on a near-global scale with fine resolution (90 m) to generate the most complete high-resolution digital topographic database of Earth (Farr et al., 2007). Meanwhile, Advanced Very High Resolution Radiometer (AVHRR) data provided the longest seasonal records of land surface that enabled us to examine continuous changes of vegetation production. These multi-sensor data assisted us our analysis of the process of soil salinization and its feedbacks to climate.

3.2.1 *Landsat data and preprocessing*

Five cloud-free scenes of Landsat MSS (Multispectral Scanner), TM (Thematic Mapper), and ETM+ (Enhanced Thematic Mapper Plus) over the study area were collected from 1979 to 2009. The acquisition dates of Landsat scenes were close to each other, ensuring that seasonal characteristics were constant and comparable (Table 1). In this study, Landsat series images were used to track the changes of land surface and evaluate the energy budget by comparing

Table 1. Parameters of the Landsat images used in the analysis of soil salinization in a semi-arid region of China.

Serial Number	Sensor	Path/Row	Acquisition time
1	Landsat-3 MSS	129/29	1979-8-24
2	Landsat-5 TM	120/29	1992-9-18
3	Landsat-7 ETM+	120/29	1999-11-1
4	Landsat-7 ETM+	120/29	2002-10-8
5	Landsat-5 TM	120/29	2009-7-15

the albedos of different land covers.

The digital number (DN) data was converted to at-sensor spectral radiance (L) using Eq. (2):

$$L = G \times Q \times F \,, \tag{2}$$

where G is rescaled gain in w m^{-2} $sr^{-1}\mu m^{-1}$, F is rescaled bias in w m^{-2} sr^{-1} μm^{-1}, and Q is the quantized calibrated pixel value in DN. Then L was further converted to reflectance (R) using Eq. (3):

$$R = \frac{\pi \times L \times d^2}{E \times \cos\theta_s} \,, \tag{3}$$

where R is unitless planetary reflectance, L is spectral radiance at the sensor's aperture, d is the distance between the Earth and the Sun in astronomical units, E is mean solar exoatmospheric irradiance, θ_s is solar zenith angle in degrees (Landsat Project Science Office, 2002).

3.2.2 *Long-term series of vegetation index*

The GIMMS (Global Inventory Modeling and Mapping Studies) dataset is a bimonthly normalized difference vegetation index (NDVI) product that has been derived from NOAA AVHRR sensors since 1981 (8 km spatial resolution). NDVI is calculated from spectral reflectance in red (R_{red}, 0.58–0.68 mm) and near infrared (R_{nir}, 0.725–1.1 mm) bands [NDVI = $(R_{nir}–R_{red})/(R_{nir}+R_{red})$] (Goward et al., 1991). This new GIMMSg3 dataset from 1981 to 2008 uses the Sea-Viewing Wide-Field-of-View Sensor (SeaWiFS) for calibration among sensors (Bhatt et al., 2010). The NDVI value roughly indicates plant photosynthesis activities of a given pixel; a higher NDVI value means greater vegetation growth. The dataset is derived from imagery obtained from the AVHRR instrument onboard the NOAA satellite series. The GIMMSg3 dataset is a NDVI dataset that has been corrected for calibration, view geometry, volcanic aerosols, and other effects not related to vegetation change (Tucker et al., 2005).

Time-integrated NDVI (TI-NDVI) is the cumulative value of NDVI recorded during each growing season. It reflects accumulated vegetation activity within a year. The growing season was defined as the period when the NDVI time series curve started to turn in spring (Goward et al., 1991; Jia et al., 2002). Here we defined a value of 0.16 from local seasonal curves as the threshold, based on the local phenology records in recent years. In this study, TI-NDVI was considered as a proxy of the ecosystem's ability to sequestrate carbon. Potential influence of soil salinization on regional climate was evaluated by diagnosing its long-term change in salt-affected areas.

3.2.3 *Spatial pattern of albedo*

Land cover change such as soil salinization influences the solar energy absorbed by the land surface. The albedo, representing the fraction of backscattered solar radiation (Pinty et al., 2010), was employed to determine the shortwave energy budget between land surface and atmosphere. The spatial distribution of albedo (A) from narrow band to broad band was calculated using Liang's method (Liang, 2000):

$$\begin{aligned} A = {} & 0.356\rho_1 + 0.130\rho_3 + 0.373\rho_4 + \\ & 0.085\rho_5 + 0.072\rho_7 - 0.0018 \,, \end{aligned} \tag{4}$$

where ρ_1, ρ_3, ρ_4, ρ_5, and ρ_7 are the reflectance bands in LANDSAT TM5/ETM$^+$: blue-green band (450–515 nm), red band (630–690 nm), near-infrared band (775–900 nm), mid-infrared band (1550–1750 nm), and mid-infrared band (2090–2350 nm).

3.3 *Change detection based on remote-sensing classification*

Supervised classification is a widely used method in extraction of land cover information. According to the field survey and local land use records, we performed a supervised classification (maximum likelihood) to acquire land cover information from Landsat image data. We performed spectral measurements over typical land cover types in our field survey. Based on these spectral characters, we selected training pixels for supervised classification. However, regions with the same land-cover type may have different spectral characteristics; therefore, some classes were separated into several subclasses to get more homogeneous pixels in a given category. For example, water bodies were separated into two subclasses: deep-water ponds and shallow-water ponds. We combined the subclasses and performed accuracy assessments of our classifications. The pixel clusters in each image were grouped into seven land cover categories: croplands, grasslands, woodlands, residential areas, salt-affected soils, water bodies, and wetlands. Land cover maps for 1979, 1992, 1999, 2002, and 2009 were overlaid two at a time, and subsequent GIS analyses were performed by applying simple image differencing. Two subsets were also created over our study area: Xianghai and Zhijian. Xianghai was chosen as a representative area of surface-water-dominated landscape, while Zhijian was chosen as an area representative of salt-affected soils. The alterations of salt-affected soils and water bodies in the Xianghai and Zhijian subsets in the period from 1979 to 2009 were detected and characterized. In addition, both the distribution and temporal changes of salt-affected soils and water bodies were analyzed.

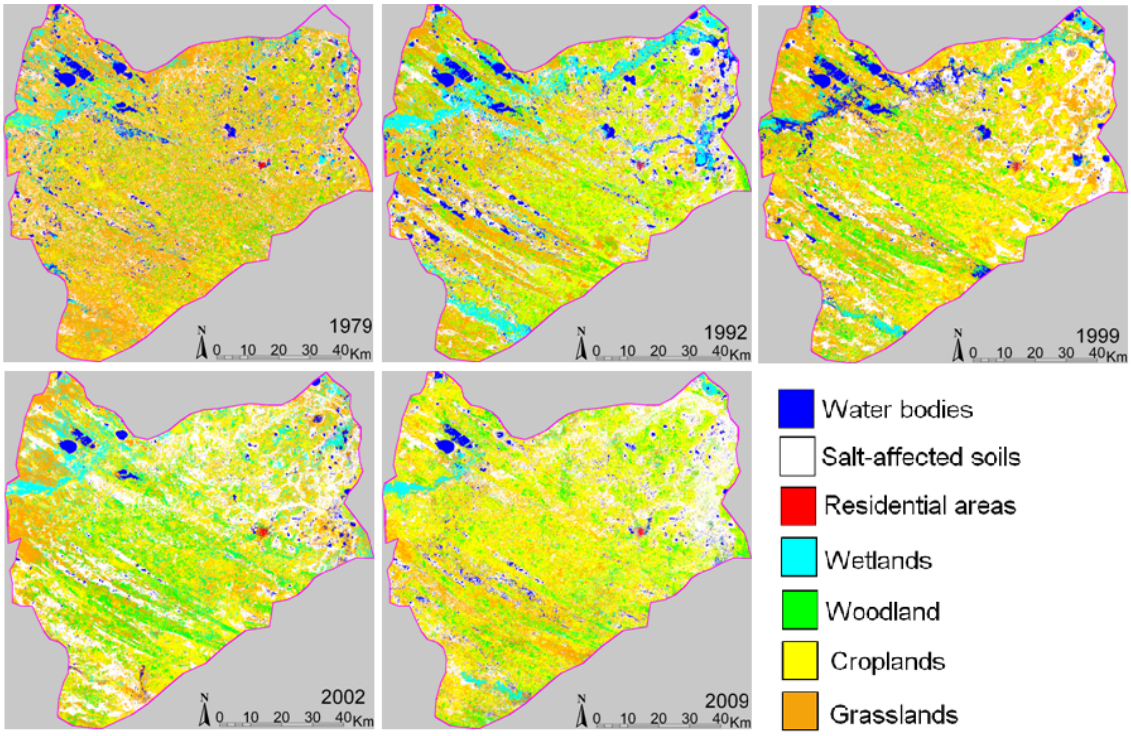

Fig. 2. Landcover classification of 1979 Multi-spectral Scanner (MSS), 1992 Thematic Mapper (TM), 1999 Enhanced Thematic Mapper Plus (ETM+), 2002 (ETM+), and 2009 (TM) of the study area.

Table 2. Accuracy assessment of Landsat image classification.

Class	1979	1992	1999	2002	2009
Water bodies (%)	95.65	97.48	94.79	94.82	95.33
Grasslands (%)	75.49	85.22	85.15	93.72	91.64
Croplands (%)	83.66	86.00	88.73	91.00	89.25
Woodlands (%)	85.71	86.59	92.47	96.32	92.24
Wetlands (%)	82.86	98.31	85.76	68.34	85.63
Residential areas (%)	68.15	63.31	67.64	80.35	76.35
Salt-affected soils (%)	88.71	92.33	95.76	94.20	95.29
Total accuracy (%)	77.04	92.60	91.55	90.06	91.25

4. Results

Main land cover types of the study area were classified into the seven categories mentioned above with five scenes of Landsat data from 1979–2009 (Fig. 2). The results of the classifications were validated with the areas surveyed in our field studies, i.e., the ground-truth areas. The accuracy of the MSS image from 1979 was relatively lower than the others. MSS uses fewer bands to extract information and has lower spatial resolution, which likely contributed to this lower accuracy. The water bodies and salt-affected soils, which had relative unique spectrum, performed at higher accuracy and at a higher kappa index (index of agreement) than the other land cover types. The residential areas with highly heterogeneous land surface exhibited the lowest accuracy and the lowest kappa index (Table 2). In general, the accuracy of classification can be accepted.

4.1 *Changes in areas affected by soil salinization*

Most of the land cover categories had undergone remarkable changes over the 30 years considered in our study (Fig. 2). Large areas of natural vegetation such as wetland and grassland were converted to farmland. The regression analysis show that the salt-affected soils had a significant linearly increasing trend (p=0.037) and that the water bodies had a slight linearly decreasing trend (p=0.383) over these 30 years. The extent of

Table 3. Areas of salt-affected soils and water bodies over case study areas from 1979 to 2009.

	Tongyu (8496 km^2)		Xianghai (258 km^2)		Zhijian (527 km^2)	
Year	water bodies	salt-affected soils	water bodies	salt-affected soils	water bodies	salt-affected soils
1979	344.72	1504.42	57.93	21.09	17.66	99.76
1992	570.70	1679.62	57.98	29.77	47.82	171.84
1999	422.32	1753.67	69.96	17.48	13.04	194.04
2002	176.86	2269.18	35.58	37.98	16.20	251.48
2009	258.21	2073.75	57.90	46.37	15.13	242.74

salt-affected soils increased along with the reduction of water bodies (Table 3).

For the entire study area, the rate of soil salinization was 23.39 km^2 yr^{-1}. In 1979, the area of salt-affected soil was 1504.42 km^2, but in 1999 it expanded to 1753.67 km^2 and to 2073.75 km^2 in 2009. The rate of salinization was 12.46 km^2 yr^{-1} from 1979 to 1999 and 35.56 km^2 yr $^{-1}$ from 1999 to 2009 (Table 3). Soil salinization accelerated in the last 10 years we studied. Water bodies, by contrast, underwent a decreasing trend (-7.06 km^2 yr^{-1}) in their area over the 30 studied years.

Two subsets, Xianghai and Zhijian, were chosen to analyze the variation of soil salinization and water bodies in four periods (1979 to 1992, 1992 to 1999, 1999 to 2002 and 2002 to 2009). In Xianghai, the extent of salt-affected soils had increased over the 30 study years (Fig. 3a, Table 3), and the expansion of salinized area was concentrated around water bodies and wetlands where the groundwater was close to the surface. Meanwhile, the areas of water bodies shrank, and much of the additional dry area was converted to salinized soil. In Zhijian, the extent of salt-affected soils increased over the 30 studied years, and the expansion was concentrated around overgrazed grasslands and lower areas that favored waterlogging. The water body for Zhijian shrank from 1979 to 2009 (Fig. 3b; Table 3). The white areas in the figure represent the salt-affected soils that did not change in terms of coverage over this period. These areas were considered to be more seriously salinized than the red areas that changed from other land cover types; they represent seriously salt-affected soils. The severity of salinization became higher over large areas during the four periods listed in Table 4. As indicated, the salt-affected soils increased not only in coverage but also in severity. The areas of seriously salt-affected soil in Zhijian increased and occupied about 32% of the area from 2002 to 2009 (170.75 km^2 vs. 526.79 km^2).

Table 4. Areas of seriously salt-affected soils over case study areas from 1979 to 2009.

Period	Xianghai	Zhijian
1979–1992 (km^2)	6.00	51.86
1992–1999 (km^2)	11.86	118.75
1999–2002 (km^2)	13.87	152.11
2002–2009 (km^2)	24.18	170.75

The salt-affected soils were mainly distributed in the northeastern part of the study area where the elevation was relatively lower than surrounding areas (Fig. 4). The water bodies were mainly distributed in the northwestern part of the study area. The fractions of salt-affected soils showed an increasing trend in lower-elevation areas and a decreasing trend in higher-elevation areas from 1979 to 2009 (Fig. 4). This indicates that lower elevation areas might be prone to waterlogging and that the high evaporation likely enhanced the accumulation of alkaline and salt in top soils, causing larger areas to be affected by salinization.

4.2 *Causes of soil salinization*

The changing climate is an important factor causing soil salinization. Because none of the water supply was from surface runoff in the study area, the enhancing aridity and weakening precipitation due to annual and summer warming trends (Figs. 5a, b) exhibited a climate tendency toward higher water deficits, which in turn reduced the coverage of water bodies and accelerated the salinization of soils. In the study area, soil salinization was highly correlated to water bodies. The hydrologic conditions are likely to have a direct impact on soil salinization. From 1979 to 2009, 51.55% of water bodies changed to salinized soils in the study area. In wet years, more precipitation can dissolve the salt accumulated on the surface of ground, increasing water bodies and reducing the area of soil salinization (Hayley et al., 2009). By contrast, in dry years, more ground water was transported upward, causing more salt to accumulate on the surface, reducing the area of water bodies, and increasing salt-affected soils. Hence, the salt-affected soils were mainly outlined near water bodies such as lakes, ponds, and rivers.

Meanwhile, human disturbances also had a crucial role in accelerating the rate of soil salinization. When the number of livestock and/or stocking rate exceed-

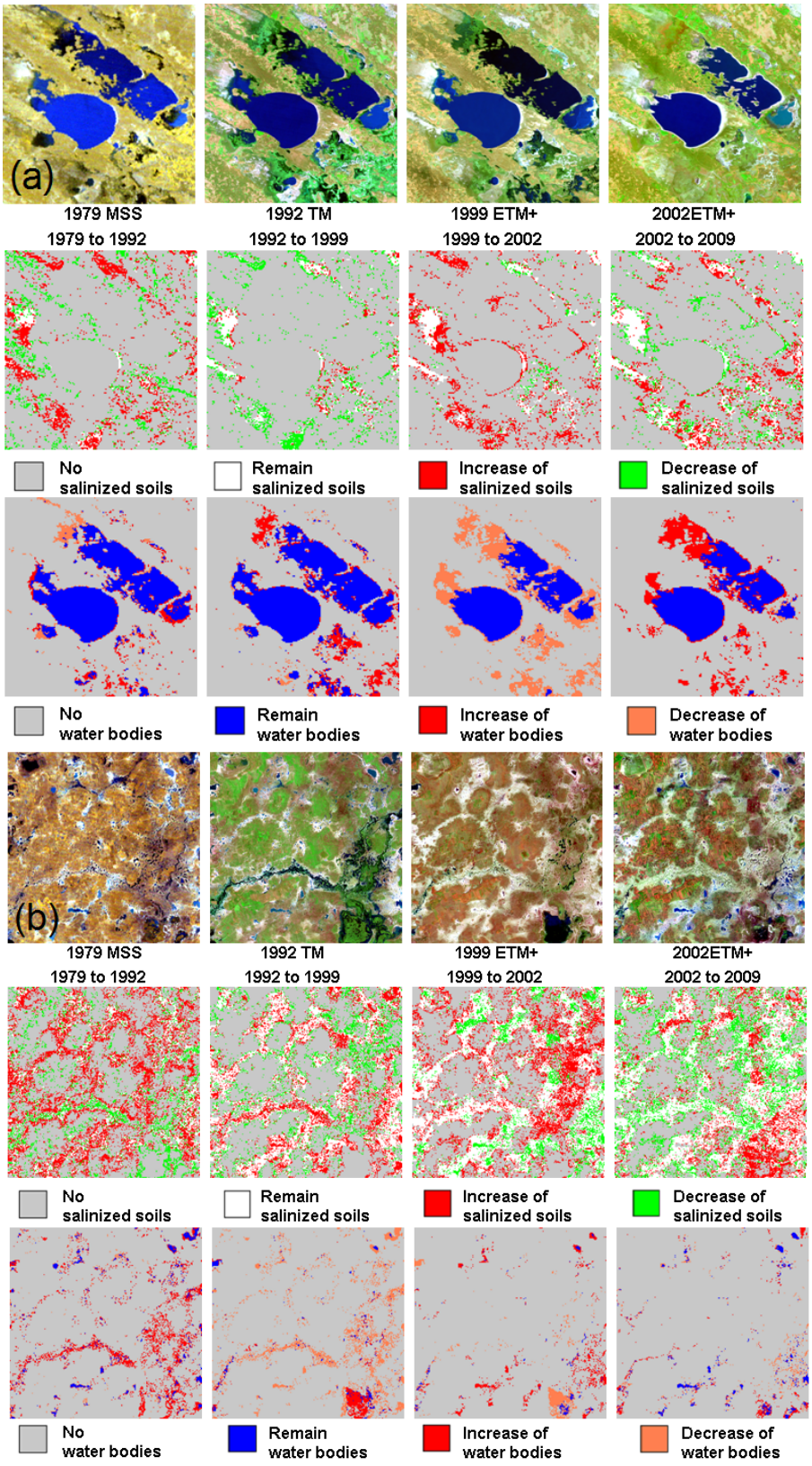

Fig. 3. Variation of salinized soils and water bodies of (a) Xianghai, representing water bodies, and (b) Zhijian representing salt-affected soils, in the 30 studied years.

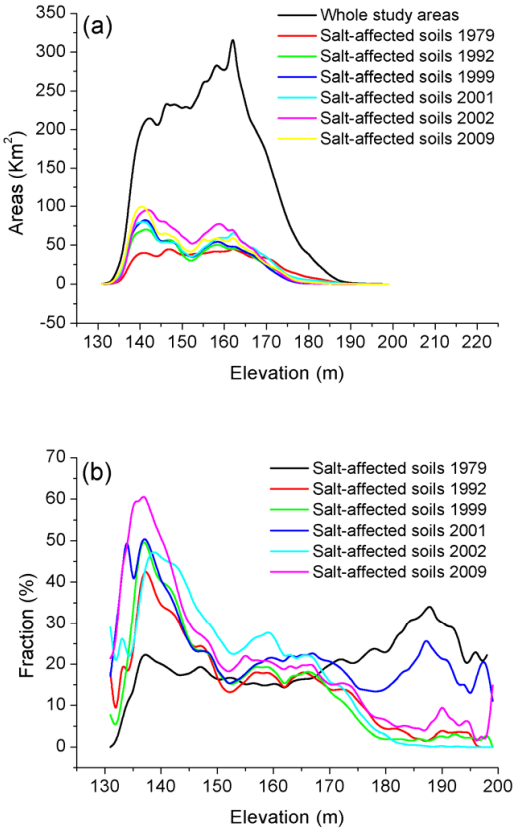

Fig. 4. (a) Area distribution and (b) fraction cover of salt-affected soils along the elevation.

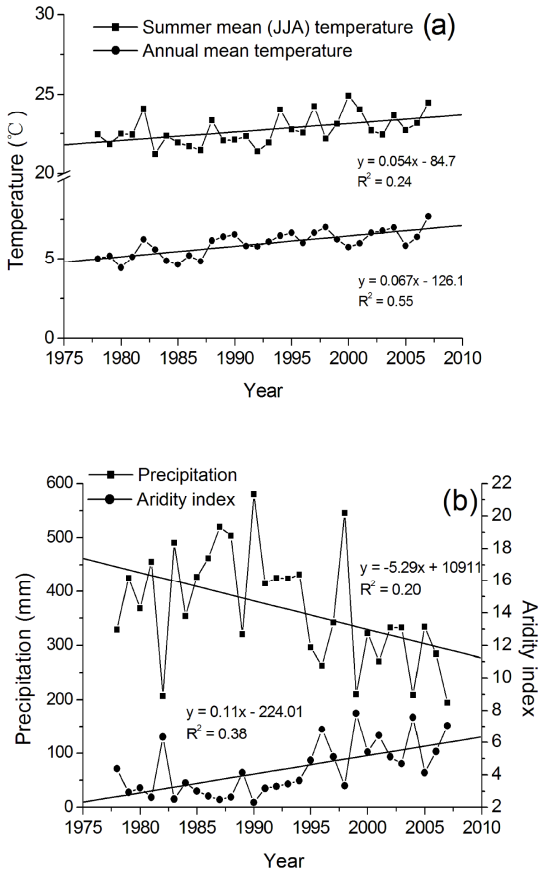

Fig. 5. Interannual variations of (a) average summer (JJA) and annual mean temperature, and (b) precipitation and aridititity index from 1978 to 2007 in the study area.

ed the carrying capacity of grasslands, grasslands were degraded. From 1979 to 2009, 21.47% of natural grassland changed to salinized soil. Further, the rapid conversion of natural grassland into irrigated cropland greatly raised the demands for groundwater irrigation in recent 30 years (Fig. 6). In the same period, 46.75% of natural grassland was cultivated for cropland. Cropland occupied much of the available groundwater and enlarged the water deficit of other natural vegetation. Furthermore, the local groundwater used for irrigation was rich in sodium, magnesium, calcium, and carbonates (Zhang et al., 2007); therefore, it provided a perfect source for soil salinity once exposed on the land surface. As a result, a large area of secondary salt-affected soils was induced, and the slightly salt-affected soils were aggravated. This cultivation occupied much of the available ground water and aggravated the process of soil salinization.

In general, the natural driving factor of salinization is the aridification of climate. Relatively flat terrain favors waterlogging, while continuous drought favors upward movement of soil water and accumulation of saline and calcium on the land surface. Meanwhile, human activities such as overgrazing, cultivation of grassland, and groundwater irrigation also play a crucial role in accelerating soil salinization.

4.3 *Effects of soil salinization on climate*

4.3.1 *Influence of carbon sequestration*

The feedbacks of soil salinization to climate in term of carbon sequestration were assessed by examining the changes in TI-NDVI derived from the AVHRR dataset over a similar study period with Landsat coverage (Fig. 7). Because much of the natural vegetation was converted to high-production cropland and the decadal warming extended the length of the growing season in northern China (Fang et al., 2004), the annual accumulated vegetation greenness (TI-NDVI) increased from 1982 to 2008 in the study area, indicated an increasing trend of vegetation production to the whole study area. However, at a more local scale in Zhijian, which was mainly occupied by natural grassland and salinized soils, wasn't influenced by cultiva-

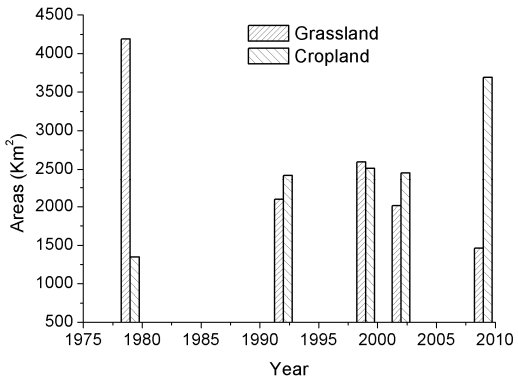

Fig. 6. Areas variations of grassland and cropland over the study areas from 1979 to 2009.

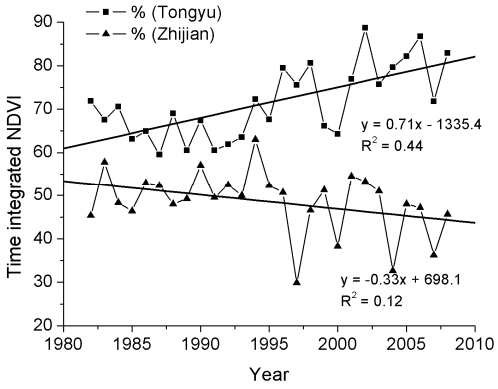

Fig. 7. Changes of time integrated NDVI (TI-NDVI) from 1982 to 2006 in Tongyu region and its two subsets: Xianghai and Zhijian.

tion and present a negative trend of vegetation production. Therefore, the salinization of soils can limit plant water use efficiency and photosynthesis, and therefore can reduce the amount of carbon sequestrated by the terrestrial ecosystem.

4.3.2 *Influence of radiation balance*

Surface albedo varied with land cover types. Water bodies and salinized soils had the lowest and highest surface albedos, respectively (Fig. 8.). The albedo of salinized soils was 6%–21% higher than average value. Conversion of cropland and natural grassland to salinized bare soil can therefore reduce surface absorption of solar radiation and further modify energy balance between land and atmosphere.

In seasonality, albedo was also controlled by water condition. It was lower during the wet season (e.g., July 2009) and higher during the dry season (e.g., November 1999). Transition periods such as September 1992, and October 2002 represent the median albedo.

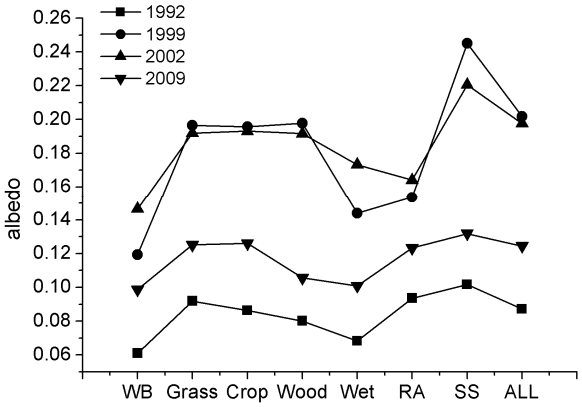

Fig. 8. Changes of albedo for different land cover types in Tongyu. WB = water bodies; Grass = grasslands; Crop = croplands; Wood = woodlands; Wet = wetlands; RA = residential areas; SS = salt-affected soils; ALL = all land cover types.

4.4 *Implications*

As a key CEOP reference site, Tongyu provided flux data between land and atmosphere used to model and validate the process of land surface. The flux data was measured using the eddy covariance (EC) method, representing a scale of hundreds of square meters. However, at a larger scale, such as a regional scale, the land cover types around the stations underwent significant changes during the later years of our study. These changes altered both the land surface processes and the interactions between land and atmosphere. Further, the representativeness of EC flux measurement was also largely affected by these changes. It is difficult and often inaccurate to up-scale field observations to a regional scale directly over a heterogeneous landscape.

In addition, we considered the rapid and continuous change of land cover types in the study area. The conversions of land cover significantly changed the energy and water balance between land and atmosphere. A static land cover map might not be suitable for climate modeling. We strongly recommend that dynamic land cover maps with fine spatial resolution be considered in regional climate models to reduce the uncertainties in simulation and projection.

5. Conclusion

In this study, we analyzed multi-sensor satellite data combined with field survey data to examine the spatial and temporal changes in soil salinization. Our analysis indicates that the salt-affected soils increased not only in extent but also in severity over the study period. The salt-affected soils were concentrated in

basins and foothills in terms of microtopography. Decreases in precipitation and increases in aridity due to decadal warming provided favorable conditions for soil salinization. Meanwhile, land-use practices also had a crucial role in accelerating soil salinization. The conversion of cropland from natural vegetation greatly increased the demand for groundwater irrigation and aggravated the process of soil salinization. Soil salinization not only reduced the vegetation production but also reduced the absorbed solar radiation. These significant changes in land cover during the 30 years of our study period consequently affected the energy and water balance between land and atmosphere. We strongly suggest that dynamic land cover maps with fine spatial resolution be considered in regional climate models.

Acknowledgements. This study was supported by the National Basic Research Program of China (Grant No. 2009CB723904), the National Natural Science Foundation of China (Grant No. 41105076), the National Key technology R & D program (Grant No. 2012BAC22B04) and the Strategic Priority Research Program of the Chinese Academy of Sciences (Grant No. XDA05090201). We would like to thank China National Meteorological Information Centre for providing climate data of the study area.

REFERENCES

Abuzar, M., A. McAllister, and M. Morris, 2001: Classification of seasonal images for monitoring irrigated crops in a salinity-affected area of Australia. *Int. J. Remote Sens.,* **22**, 717–726.

Bhatt, U. S., and Coauthors, 2010: Circumpolar arctic tundra vegetation change is linked to sea ice decline. *Earth Interactions*, **14**, paper No.8.

Chen, S., and P. Rao, 2008: Land degradation monitoring using multi-temporal Landsat TM/ETM data in a transition zone between grassland and cropland of northeast China. *Int. J. Remote Sens.*, **29**, 2055–2073.

Chen, S., and Y. Zhou, 2005: Classifying depth-layered geological structures on Landsat TM images by gravity data: a case study of the western slope of Songliao Basin, Northeast China. *Int. J. Remote Sens.*, **26**, 2741–2754.

Eldeiry, A. A., and L. A. Garcia, 2008: Detecting soil salinity in alfalfa fields using spatial modeling and remote sensing. *Soil Science Society of America Journal*, **72**, 201–211.

Farr, T. G., and Coauthors, 2007: The Shuttle Radar Topography Mission. *Rev. Geophys.*, **45**, RG2004.

Fang, J. Y., S.L. Piao, J. S. He, and W. H. Ma, 2004: Increasing terrestrial vegetation activity in China, 1982–1999. *Science in China* (*C*), **147**, 229–240.

Farifteh, J., A. Farshad, and R. J. George, 2006: Assessing salt-affected soils using remote sensing, solute modeling, and geophysics. *Geoderma,* **130**, 191–206.

Farifteh, J., F. Van der Meer, C. Atzberger, and E. J. M. Carranza, 2007: Quantitative analysis of salt-affected soil reflectance spectra: A comparison of two adaptive methods (PLSR and ANN). *Remote Sens. Environ.*, **110**, 59–78.

Fernandez-Buces, N., C. Siebe, S. Cram, and J. L. Palacio, 2006: Mapping soil salinity using a combined spectral response index for bare soil and vegetation: A case study in the former lake Texcoco, Mexico. *Journal of Arid Environments*, **65**, 644–667.

Funakawa, S., and T. Kosaki, 2003: Potential risk of soil salinization in different regions of Central Asia with special reference to salt reserves in deep layers of soils. *Soil Science and Plant Nutrition*, **53**, 634–649.

Goward, S. N., B. Markham, and D. G. Dye, 1991: Normalized difference vegetation index measurements from the advanced very high resolution radiometer. *Remote Sens. Environ.*, **35**, 257–277.

Hayley, K., L. R. Bentley, and M. Gharibi, 2009: Time-lapse electrical resistivity monitoring of salt-affected soil and groundwater. *Water Resource Research*, **45**, 1–14.

Howari, F. M., 2003: The use of remote sensing data to extract information from agricultural land with emphasis on soil salinity. *Australian Journal of Soil Research*, **41**, 1243–1253.

Jia, G. J., H. E. Epstein, and D. A.Walker, 2002: Spatial characteristics of AVHRR-NDVI along latitudinal transects in northern Alaska. *Journal of Vegetation Science*, **13**, 315–326.

Landsat Project Science Office, 2002: Landsat 7 science data user's handbook. Goddard Space Flight Center. [Available at http:// landsathandbook.gsfc.nasa.gov/handbook.html.]

Li, X. Y., Z. M. Wang, K. S. Song, B. Zhang, D. W. Liu, and Z. X. Guo, 2007: Assessment for salinized wasteland expansion and land use change using GIS and remote sensing in the west part of Northeast China. *Environmental Monitoring and Assessment*, **131**, 421–437.

Liang, S. L., 2000: Narrowband to broadband conversions of land surface albedo I Algorithms. *Remote Sens. Environ.*, **76**, 213–238.

Lobell, D. B., J. I. Ortiz-Monasterio, F. C. Gurrola, and L. Valenzuela, 2007: Identification of saline soils with multiyear remote sensing of crop yields. *Soil Science Society of America Journal*, **71**, 777–783.

Masoud, A. A., and K. Koike, 2006: Arid land salinization detected by remotely-sensed landcover changes: A case study in the Siwa region, NW Egypt. *Journal of Arid Environments*, **66**, 151–167.

Metternicht, G. I., and J. A. Zinck, 1997: Spatial discrimination of salt- and sodium-affected soil surfaces. *Int. J. Remote Sens.*, **18**, 2571–2586.

Metternicht, G. I., and J. A. Zinck, 2003: Remote sensing of soil salinity: Potentials and constraints. *Remote Sens. Environ.*, **85**, 1–20.

Penman, H. L., 1948: Natural evaporation from open water, bare soil, and grass. *Proc. Roy. Soc. London* (*A*), **193**, 454–465.

Pinty, B., M. Taberner, V. R. Haemmerle, S. R. Paradise, E. Vermote, M. M. Verstraete, N. Gobron, and J. Widlowski, 2010: Global-scale comparison of MISR and MODIS Land Surface Albedos. *J. Climate*, **24**, 732–749.

Qi, S. Z., and F. Luo, 2006: Land-use change and its environmental impact in the Heihe River Basin, arid northwestern China. *Environmental Geology*, **50**, 535–540.

Shrestha, R. P., 2006: Relating soil electrical conductivity to remote sensing and other soil properties for assessing soil salinity in northeast Thailand. *Land Degradation and Development*, **17**, 677–689.

Tucker, C. J., J. E. Pinzon, M. E. Brown, D. Slayback, E. W. Pak, R. Mahoney, E. Vermote, and N. El Saleous, 2005: An extended AVHRR 8-km NDVI data set compatible with MODIS and SPOT vegetation NDVI data. *Int. J. Remote Sens.*, **26**, 4485–5598.

Wang, H. Q., Y. H. Ping, M. A. Harwella, and W. R. Huang, 2007: Modeling soil salinity distribution along topographic gradients in tidal salt marshes in Atlantic and Gulf coastal regions. *Ecological Modelling*, **201**, 429–439.

Wang, Y. G., Y. Li, and D. N. Xiao, 2008: Catchment scale spatial variability of soil salt content in agricultural oasis, Northwest China. *Environmental Geology*, **56**, 439–446.

Yang, X., K. Zhang, B. Jia, and L. Ci, 2005: Desertification assessment in China: An overview. *Journal of Arid Environments*, **63**, 517–531.

Zhang, G. X., W. Deng, Y. S. Yang, and R. B. Salama, 2007: Evolution study of a regional groundwater system using hydrochemistry and stable isotopes in Songnen Plain, northeast China. *Hydrological Processes*, **21**, 1055–1065.